AUT Journal of Civil Engineering

AUT J. Civil Eng., 5(3) (2021) 465-480
DOI: 10.22060/ajce.2021.19911.5752

# Two-Dimensional Geometrically Nonlinear Hyperelastic Wave Propagation Analysis in FG Thick Hollow Cylinders using MLPG Method

M.H. Ghadiri Rad[1], F. Shahabian[2*] , S.M. Hosseini[3]

[1] Civil Engineering Department, Quchan University of Technology, Quchan, Iran.
[2] Civil Engineering Department, Ferdowsi University of Mashhad, Mashhad, Iran.
[3] Industrial Engineering Department, Ferdowsi University of Mashhad, Mashhad, Iran.

**ABSTRACT:** The idea of using a meshless method for geometrically nonlinear problems due to its advantage of eliminating mesh distortion has been attracted many researchers. In this paper, the nonlinear wave propagation analysis in two-dimensional functionally graded (2D FG) thick hollow cylinders is studied using the meshless method. For this purpose, the meshless local Petrov-Galerkin (MLPG) method is developed for geometrically nonlinear dynamic analysis based on the total Lagrangian approach. The radial point interpolation, which possesses the delta function property, is used to construct the shape functions. Since the cylinder is assumed to have large deformations, the neo-Hookean hyperelastic model is employed for constitutive modeling of material. The incremental-iterative Newmark/Newton-Raphson technique is applied to iteratively solve the nonlinear equations of motion. The 2D FG cylinder is analyzed under uniform and non-uniform mechanical shock loading. The mechanical properties of the cylinder are assumed to vary nonlinearly through the radial and longitudinal directions which are simulated using two-dimensional volume fractions. Rayleigh damping is utilized to model energy dissipation in analyses. Numerical examples demonstrate the applicability and accuracy of the present approach in tracking the nonlinear wave propagation in two-dimensional FG thick hollow cylinders. The effects of grading patterns on the time history and wave propagation are discussed in detail.

**Review History:**

Received: Apr. 25, 2021
Revised: Nov. 09, 2021
Accepted: Nov. 11, 2021
Available Online: Dec, 03, 2021

**Keywords:**

Two-dimensional wave propagation
Meshless local Petrov-Galerkin (MLPG) method
Geometrically nonlinear problems
Two-dimensional functionally graded materials
Neo-Hookean constitutive model.

## 1- Introduction

Functionally graded materials are a new type of composite materials in which the material properties vary continuously through one or two directions to achieve the optimum properties. Recently, studying dynamic behavior and wave propagation of structures made of FGMs has attracted the attention of many researchers. For instance, Moussavi-nezhad et al. [1] developed the MLPG method for stress wave propagation in finite-length FG cylinders. The wave propagation of nano-beams/tubes made of FGMs has been analytically studied by Norouzzadeh et al. [2]. Sur et al. [3] investigated the heat transport in the functionally graded thick plate in the context of Taylor's series expansion involving memory-dependent derivative for the dual-phase-lag (DPL) heat conduction law. Aminpour et al. [4] attempted to elucidate the size-dependent behavior of functionally graded (FG) Anisotropic macro/nanoplates.

Many engineering problems can be analyzed based on linear approximations. But when the structure experiences large deformations, it is incorrect to neglect the effects of large deformations on the geometric configuration of the structure. The finite element method (FEM) has been widely used to analyze geometrically nonlinear problems [5-7]. However, in the analysis of some problems using FEM, because of its mesh-based interpolation, poor accuracy of the stress field, shear locking in modeling of thin-walled structures, mesh dependency and mesh distortion during large deformation analyses affect the solution accuracy [8]. To overcome the drawbacks of FEM, meshless techniques have been developed by researchers. In these techniques, a set of scattered nodes rather than meshes is used to discrete the problem domain and boundaries. Smooth particle hydrodynamics (SPH) [9], diffuse element method (DEM) [10], reproducing kernel particle method (RKPM) [11], element free Galerkin (EFG) [12], meshless natural neighbor Galerkin method [13], meshless local Petrov–Galerkin method (MLPG) [14] and local boundary integral equation (LBIE) [15] are the most widely used meshless methods. It should be mentioned that the main difference between these various meshless methods arises from the shape function production approaches. The stability, convergence of accuracy, and cost-efficiency of four various meshless formulations for the solution of boundary value problems in non-homogeneous elastic solids with functionally graded Young's modulus were investigated by Sladek et al. [16]. Among the meshless methods, the MLPG method due to its flexibility and simple implementation is a well-developed meshless method. Sladek et al. [16] presented a review for analysis of problems in engineering and sciences, using the MLPG method.

*Corresponding author's email: shahabf@um.ac.ir

In recent years, the meshless methods provide an efficient alternative to the finite element method for geometrically nonlinear problems. Hao et al. [17] studied on geometrically nonlinear forced vibration of FG plates under transversal and in-plane excitations with the help of Galerkin's method. Sladek et al. [18] based on Von Karman's theory, proposed a large-deformation meshless method to solve dynamic problems for Reissner–Mindlin plates with magneto-electro-elastic properties. They compared the numerical results with those obtained by the 3D FEM analyses and demonstrated that the meshless results are in good agreement with FEM. In addition, the 3D FEM needs a significantly higher number of nodes compared with the meshless method. Zhang et al. [19] presented an effective three-dimensional (3D) nonlinear explicit dynamic meshfree algorithm based on the element-free Galerkin (EFG) method using the moving least square (MLS) approximation. In their algorithm, the materials were regarded as a neo-Hookean hyper-elastic and nearly incompressible continuum. Zhang et al. [20] studied on geometrically nonlinear behavior of carbon nanotube-reinforced functionally graded (CNTR-FG) cylindrical panels under uniform transverse mechanical loading. Zhao et al. [21] based on Sander's nonlinear shell theory, extended the element-free kp-Ritz method for geometrically nonlinear analysis of plates and cylindrical shells. The comparison of their results with the reported results in other works of the literature demonstrated the efficiency of their presented solution method in handling the snap-through and snap-back in shell problems. Zhu et al. [22] adopted the MLPG method with the Kriging interpolation technique to perform a geometrically nonlinear thermo-mechanical analysis of moderately thick functionally graded plates, based on the first-order shear deformation plate theory. In their paper, both the thermal and large deformation analysis leads to nonlinear partial differential equations (PDEs) which were solved using the arc-length methods. Ghadiri Rad et al. [23] studied the geometrically nonlinear dynamic behavior of nanobeams using the element-free Galerkin (EFG) method. Mellouli et al. [24] developed a meshfree method for geometrically nonlinear analysis of 3D-shell structures based on the double director's shell theory with finite rotations.

In this paper for the first time, the MLPG method is developed for geometrically nonlinear wave propagation analysis of two-dimensional functionally graded thick hollow cylinders in which the material properties vary nonlinearly through the radial and longitudinal directions. Since the cylinder is assumed to involve large deformations, the neo-Hookean model, a hyperelastic constitutive model, is employed to obtain the nonlinear stress-strain relationship. The mechanical properties of the 2D FG cylinder are simulated using two-dimensional volume fractions. The nonlinear wave propagation of the displacement field for various FG distributions is studied in detail.

## 2- Radial point interpolation

In this section, the meshless shape function construction using the radial point interpolation method (RPIM) is briefly introduced. More details can be found in the paper by Liu and Gu [25]. RPIM is based on interpolation of the function '$u$' among a set of scattered nodes in a small local domain which affects '$u$'. Such a local domain is termed the support domain '$\Omega_s$'. Using the RPIM shape function '$\boldsymbol{\Phi}$'', the approximation of '$u$' in support domain of point '$\mathbf{x}$' can be expressed concerning its nodal values vector '$\mathbf{U}_s$'.

$$u = \boldsymbol{\Phi}\,\mathbf{U}_s \tag{1}$$

The RPIM shape function can be obtained as:

$$\boldsymbol{\Phi} = \mathbf{R}^{\mathrm{T}}(\bar{r})\mathbf{R}_Q^{-1} \tag{2}$$

Where $\mathbf{R}^{\mathrm{T}}(\bar{r})$ is the radial basis function (RBF) matrix and $\mathbf{R}_Q$ is composed of nodal values of radial basis function (RBF):

$$\mathbf{R}^{\mathrm{T}}(r) = \begin{bmatrix} R_1(\bar{r}) & R_2(\bar{r}) & \cdots & R_n(\bar{r}) \end{bmatrix} \tag{3}$$

$$\mathbf{R}_Q = \begin{bmatrix} R_1(\bar{r}_1) & R_2(\bar{r}_1) & \cdots & R_n(\bar{r}_1) \\ R_1(\bar{r}_2) & R_2(\bar{r}_2) & \cdots & R_n(\bar{r}_2) \\ \vdots & \vdots & \ddots & \vdots \\ R_1(\bar{r}_n) & R_2(\bar{r}_n) & \cdots & R_n(\bar{r}_n) \end{bmatrix} \tag{4}$$

Where the term '$n$' is the number of nodes located in the support domain. In this paper, the multiquadrics (MQ) radial basis function is used, which is defined as follows [1].

$$R_i(\bar{r}) = \left[(r-r_i)^2 + (z-z_i)^2 + c^2\right]^q = \left(\bar{r}^2 + c^2\right)^q \tag{5}$$

The parameters '$q$' and '$c$' are determined to be equal to 0.5 and the average nodal spacing, respectively.

## 3- Nonlinear formulation

### 3- 1- Kinematics

Fig. 1 shows a body with finite deformation. The body occupies the domain $\Omega_0$ at the initial state. After the application of the loads, the body deforms and occupies a new domain $\Omega$ at the current configuration. The position vectors in the initial and current configurations are denoted by $\mathbf{x}$ and $\mathbf{x}$, respectively.

In the total Lagrangian description, the motion of the body is referred to as the initial (un-deformed) configuration. The current coordinate can be expressed in terms of initial coordinates using the following equation.

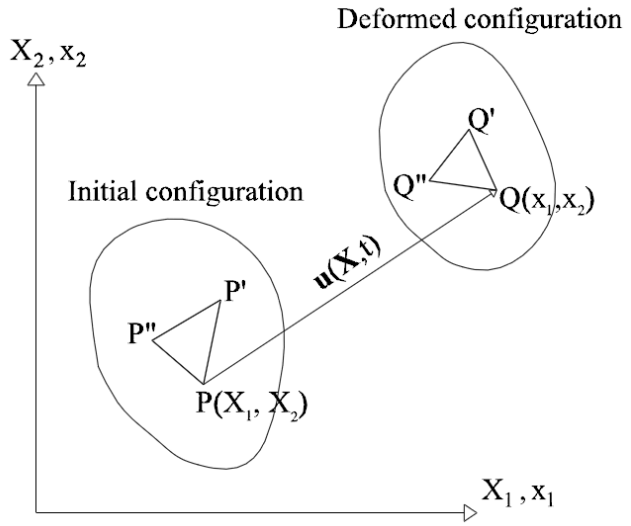


**Fig. 1. Initial and deformed configuration of a body with finite deformations.**

$$\mathbf{x} = \mathbf{X} + \mathbf{u}(\mathbf{X}, t) \tag{6}$$

Where $\mathbf{u}$ is the displacement vector. The deformation gradient is one of the key quantities in finite deformation analysis which maps a differential line element from the initial (material) configuration to the current (spatial) configuration and is given in convective description as

$$F_{ij} = \frac{\partial x_i}{\partial X_j} = \delta_{ij} + \frac{\partial u_i}{\partial X_j} = \delta_{ij} + u_{i,j} \tag{7}$$

Thus, the deformation gradient tensor can be used to obtain the change in length and direction of a differential line element during a finite deformation.

$$dx_i = F_{iI}\, dX_I \tag{8}$$

The components of the deformation gradient tensor in the polar coordinate system considering axisymmetric conditions are given by:

$$F_{rr} = 1 + u_{r,r},\ F_{\theta\theta} = 1 + \frac{u_r}{r},\ F_{zz} = 1 + u_{z,z},\ F_{rz} = u_{r,z},\ F_{zr} = u_{z,r} \tag{9}$$

The variation of deformation gradient can be derived using Eqs. (1) and (7).

$$\mathbf{\Delta F} = \begin{Bmatrix} \Delta F_{rr} \\ \Delta F_{\theta\theta} \\ \Delta F_{zz} \\ \Delta F_{rz} \\ \Delta F_{zr} \end{Bmatrix} = \begin{bmatrix} \phi_{i,r} & 0 \\ \phi_i / r & 0 \\ 0 & \phi_{i,z} \\ \phi_{i,z} & 0 \\ 0 & \phi_{i,r} \end{bmatrix} \begin{bmatrix} \Delta u_r \\ \Delta u_z \end{bmatrix}, \quad \mathbf{\Delta F} = \mathbf{B}^l\, \mathbf{\Delta u} \tag{10}$$

### 3- 2- Nonlinear strain-displacement relationship

The Green-Lagrange strain tensor is a strain measure defined in the initial configuration. At the initial configuration, the right Cauchy-Green deformation tensor $C_{ij}$ is introduced as

$$C_{ij} = F_{ki}\, F_{kj} \tag{11}$$

The Green-Lagrange strain tensor is given by

$$C_{ij} = F_{ki}\, F_{kj} \tag{12}$$

Using the chain rule, the following incremental equation can be derived from Eq. (12).

$$\Delta\varepsilon_{ij} = F_{ki}\, \Delta F_{kj} + \Delta F_{ki}\, F_{kj} \tag{13}$$

Expanding the above equation gives the matrix form of Green–Lagrange strain tensor variation in the polar coordinate system.

$$\mathbf{\Delta\varepsilon} = \hat{\mathbf{F}}\, \mathbf{\Delta F} \tag{14}$$

Where

$$\varepsilon_{zz} \quad \gamma_{rz} \Big]^T,\ \gamma_{rz} = \varepsilon_{rz} + \varepsilon_{zr} \tag{15}$$

$$\hat{\mathbf{F}} = \begin{bmatrix} F_{rr} & 0 & 0 & 0 & F_{zr} \\ 0 & F_{\theta\theta} & 0 & 0 & 0 \\ 0 & 0 & F_{zz} & F_{rz} & 0 \\ F_{rz} & 0 & F_{zr} & F_{rr} & F_{zz} \end{bmatrix} \tag{16}$$

Substitution Eq. (10) into Eq. (14) yields:

$$\boldsymbol{\Delta\varepsilon} = \left(\hat{\mathbf{F}}\,\mathbf{B}^{l}\right)\boldsymbol{\Delta u} = \mathbf{B}^{nl}\,\boldsymbol{\Delta u} \tag{17}$$

Where

$$\mathbf{B}^{nl} = \begin{bmatrix} F_{rr}\,\phi_{i,r} & F_{zr}\,\phi_{i,r} \\ F_{\theta\theta}\,\phi_i / r & 0 \\ F_{rz}\,\phi_{i,z} & F_{zz}\,\phi_{i,z} \\ F_{rr}\,\phi_{i,z} + F_{rz}\,\phi_{i,r} & F_{zr}\,\phi_{i,z} + F_{zz}\,\phi_{i,r} \end{bmatrix} \tag{18}$$

## 4- Constitutive Equation

### 4- 1- Stress-strain relationship

Hyper-elastics are elastic materials with strongly nonlinear stress-strain relation. These materials are characterized by introducing a strain energy density function '$W$'. Strain energy is the mechanical work required in a reversible process to produce a particular state of strain. For an isotropic material, '$W$' can be expressed as a function of invariants of the right Cauchy-Green deformation tensor.

$$W = W\left(I_1, I_2, I_3, \mathbf{X}\right) \tag{19}$$

Where

$$I_1 = \mathbf{tr}\left(\mathbf{C}\right) = \mathbf{I}\,\mathbf{C} = C_{11} + C_{22} + C_{33},\ I_2 = \\ = \mathbf{tr}\left(\mathbf{C}\,\mathbf{C}\right) = \mathbf{C}\,\mathbf{C},\ I_3 = \mathbf{det}\left(\mathbf{C}\right) = J^2 \tag{20}$$

Where '$\mathbf{I}$' is the unit matrix. For hyper-elastic materials, the second Piola-Kirchoff stress is the first derivative of the strain energy density function concerning the Green-Lagrange strain.

$$\mathbf{S} = \frac{\partial W}{\partial \boldsymbol{\varepsilon}} = 2\frac{\partial W}{\partial \mathbf{C}} = 2\left(\frac{\partial W}{\partial I_1}\frac{\partial I_1}{\partial \mathbf{C}} + \frac{\partial W}{\partial I_2}\frac{\partial I_2}{\partial \mathbf{C}} + \frac{\partial W}{\partial I_3}\frac{\partial I_3}{\partial \mathbf{C}}\right) \tag{21}$$

Several approaches are available for constitutive modeling of hyper-elastic based on the definition of strain energy functions. Among these, the neo-Hookean is one of the most used models. The neo-Hookean model is represented by the following stored energy function [26]:

$$W = \frac{\mu}{2}\left(I_1 - 3\right) - \mu\,\mathbf{ln}\,J + \frac{\lambda}{2}\left(\mathbf{ln}\,J\right)^2 \tag{22}$$

Where '$\lambda$', '$\mu$' are Lame constants which are equal to '$\mu/2$' and '$\nu E/\left((1+\nu)(1-2\nu)\right)$', respectively. Using Eqs. (21) and (22), the second Piola-Kirchoff stress matrix concerning the initial configuration in the neo-Hookean model can be obtained as:

$$\mathbf{S} = \lambda\,\mathbf{ln}\,J\,\mathbf{C}^{-1} + \mu\left(\mathbf{I} - \mathbf{C}^{-1}\right) \tag{23}$$

### 4- 2- 2D functionally graded materials

FGMs are a special class of composites that have gained widespread applications in aircraft and space vehicle structures, defense industries, nuclear reactors, the transportation sector, etc., which are used to increase functional performance enhanced by the desired variational properties of the material combinations. This continuous variation prevents the stress concentrations at the boundary of different materials. Two-dimensional FGMs are usually made by a continuous combination of three or four distinct material phases. In this paper, the inner surface of the cylinder is considered to be made of two kinds of a material denoted by 'c1' and 'c2', and the outer surface is made of two kinds of another material denoted by 'm1' and 'm2'. The properties of the basic constituents of the FG cylinder can be found in Table 1.

**Table 1. Basic constituents of 2D FG cylinder.**

| Constituents | $E\left(GPa\right)$ | $\rho\left(kg/m^3\right)$ |
|---|---|---|
| c1 | 440 | 3210 |
| c2 | 300 | 3470 |
| m1 | 115 | 4515 |
| m2 | 69 | 2715 |

The material properties at an arbitrary point, in the 2D-FGM cylinder, can be simulated as follows [1].

$$P\left(r,z\right) = P_{c1}\,V_{c1} + P_{c2}\,V_{c2} + P_{m1}\,V_{m1} + P_{m2}\,V_{m2} \tag{24}$$

The term '$P\left(r,z\right)$' can be considered as a modulus of elasticity and density. The presented volume fractions vary as two-dimensional nonlinear functions.

$$V_{c1}=(1-\lambda_r)(1-\lambda_z),\ V_{c2}=(1-\lambda_r)\lambda_z, V_{m1}=\lambda_r(1-\lambda_z), V_{m2}=\lambda_r\lambda_z \tag{25}$$

$$\lambda_r=\left(\frac{r-r_i}{r_o-r_i}\right)^{n_r},\quad \lambda_z=\left(\frac{z}{L}\right)^{n_z} \tag{26}$$

## 5- Meshless Technique

In the case of axisymmetric problems, using the polar coordinate system simplifies the formulations. Considering axisymmetric conditions, the stress components must satisfy the following differential equations of motion in radial and longitudinal directions at the current configuration:

$$\sigma_{rr,r}+\sigma_{zr,z}+\frac{\sigma_{rr}-\sigma_{\theta\theta}}{r}-\rho u_{r,tt}=0 \tag{27}$$

$$\sigma_{zz,z}+\sigma_{rz,r}+\frac{\sigma_{rz}}{r}-\rho u_{z,tt}=0 \tag{28}$$

Where $\sigma_{ij}$ are the components of the Cauchy (real) stress tensor. In these equations, the tensor notation is used to denote partial derivatives. The differential forces at the current configuration can be expressed as:

$$dT_i=\sigma_{ji}\,n_j\,dS \tag{29}$$

Where '$n_j$' is '$j$' directional component of a unit vector normal to the current surface '$dS$'. To get the forces at the current configuration concerning the initial configuration, the following relations between the parameters at the initial and current configuration are defined.

$$\sigma_{ij}=\frac{1}{|F|}F_{ik}\,P_{kj},\quad n_{0i}=F_{ik}\,n_k,\quad dS=|F|dS_0 \tag{30}$$

In these equations, zero subscripts refer to the parameters at the initial configuration and $P_{ij}$ are the components of the 1st Piola–Kirchhoff stress tensor. Substitution Eq. (30) into Eq. (29) leads to:

$$dT_i=P_{ji}\,n_{0j}\,dS_0 \tag{31}$$

Comparing this equation with Eq. (29) indicates that for obtaining the current forces concerning the initial configuration, the Cauchy stress tensor must be replaced by the 1st Piola-Kirchhoff stress tensor. Making this replacement into Eqs. (27) and (28), one can write the weak form of the equation of motion concerning the initial configuration.

$$\int_{\Omega_{Q_0}}\left(P_{rr,r}+P_{zr,z}+\frac{P_{rr}-P_{\theta\theta}}{r}-\rho_0 u_{r,tt}\right)W_r\,d\Omega_Q=0 \tag{32}$$

$$\int_{\Omega_{Q_0}}\left(P_{zz,z}+P_{rz,r}+\frac{P_{rz}}{r}-\rho_0 u_{z,tt}\right)W_z\,d\Omega_Q=0 \tag{33}$$

Where $W_r$ and $W_z$ are the test functions in radial and longitudinal directions, respectively. Applying Gauss divergence theorem to these equations, the governing equations take the following forms:

$$\int_{\Omega_{Q_0}}\mathbf{W}'\mathbf{P}\,d\Omega_Q-\int_{\Gamma_{Q_0}}r\,\mathbf{W}\mathbf{N}\mathbf{P}\,d\Gamma_Q+\int_{\Omega_{Q_0}}r\,\mathbf{W}\rho_0\,\ddot{\mathbf{u}}\,d\Gamma_Q=0 \tag{34}$$

Where

$$\mathbf{W}'=\begin{bmatrix}rW_{r,r} & W_r & 0 & 0 & rW_{r,z}\\ 0 & 0 & rW_{z,z} & rW_{z,r} & 0\end{bmatrix},\quad \mathbf{P}^{\mathrm{T}}=\begin{bmatrix}P_{rr} & P_{\theta\theta} & P_{zz} & P_{rz} & P_{zr}\end{bmatrix} \tag{35}$$

$$\mathbf{W}=\begin{bmatrix}W_r & 0\\ 0 & W_z\end{bmatrix},\ \mathbf{N}=\begin{bmatrix}n_{r0} & 0 & 0 & 0 & n_{z0}\\ 0 & 0 & n_{z0} & n_{r0} & 0\end{bmatrix},\quad \ddot{\mathbf{u}}^{\mathrm{T}}=\begin{bmatrix}u_{r,tt} & u_{z,tt}\end{bmatrix} \tag{36}$$

The local boundary, in general, may be composed of three parts ($\Gamma_{Q_0}=\Gamma^i_{Q_0}\cup\Gamma^u_{Q_0}\cup\Gamma^t_{Q_0}$). $\Gamma^i_{Q_0}$ is the internal boundary which is located entirely inside the global domain. $\Gamma^u_{Q_0}$ and $\Gamma^t_{Q_0}$ are parts of the external boundary with prescribed essential and natural boundary conditions, respectively. Thus, Eq. (34) can be taken into account in a new form as follows.

$$\int_{\Omega_{Q_0}}\mathbf{W}'\mathbf{P}\,d\Omega_Q-\int_{\Gamma^i_{Q_0}+\Gamma^u_{Q_0}}r\,\mathbf{W}\mathbf{N}\mathbf{P}\,d\Gamma_Q+\int_{\Omega_{Q_0}}r\,\mathbf{W}\rho_0\,\ddot{\mathbf{u}}\,d\Gamma_Q=\int_{\Gamma^t_{Q_0}}r\,\mathbf{W}\overline{\mathbf{T}}\,d\Gamma_Q \tag{37}$$

The Eq. (37) is nonlinear and must be solved using an incremental/iterative procedure. To get the incremental equation of motion, the following incremental relationships can be defined during a finite deformation.

$$\mathbf{P}_{t+dt} = \mathbf{P}_t + \mathbf{\Delta P},\ \ \ddot{\mathbf{u}}_{t+dt} = \ddot{\mathbf{u}}_t + \mathbf{\Delta \ddot{u}} \tag{38}$$

Inserting Eq. (38) into Eq. (37) yields

$$\begin{aligned} &\int_{\Omega_{Q_0}} \mathbf{W}' \mathbf{\Delta P}\, d\Omega_Q - \int_{\Gamma^i_{Q_0}+\Gamma^u_{Q_0}} r\, \mathbf{W}\, \mathbf{N}\, \mathbf{\Delta P}\ d\Gamma_Q + \\ &\int_{\Omega_{Q_0}} r\, \rho_0\, \mathbf{W}\, \mathbf{\Delta \ddot{u}}\, d\Gamma_Q = \int_{\Gamma^t_{Q_0}} r\, \mathbf{W}\, \overline{\mathbf{T}}\ d\Gamma_Q \\ &- \int_{\Omega_{Q_0}} \mathbf{W}'\ \mathbf{P}_t\, d\Omega_Q + \int_{\Gamma^i_{Q_0}+\Gamma^u_{Q_0}} r\, \mathbf{W}\, \mathbf{N}\, \mathbf{P}_t\ d\Gamma_Q \\ &- \int_{\Omega_{Q_0}} r\, \rho_0\, \mathbf{W}\, \ddot{\mathbf{u}}_t\, d\Gamma_Q \end{aligned} \tag{39}$$

For each finite strain measure, there is a corresponding stress measure that is conjugate to it in the sense of virtual work. The corresponding stress to the Green-Lagrange strain is the second Piola-Kirchhoff symmetric stress. The 1st Piola-Kirchhoff stresses ($P_{ij}$) can be related to the second Piola-Kirchhoff stresses ($S_{ij}$) through the following transformation.

$$P_{ij} = S_{ik}\, F_{jk},\ \ \Delta P_{ij} = S_{ik}\, \Delta F_{jk} + \Delta S_{ik}\, F_{jk} \tag{40}$$

It is convenient to write the Eq. (40) in the following matrix form.

$$\mathbf{P} = \overline{\mathbf{F}}\, \mathbf{S},\ \ \mathbf{\Delta P} = \overline{\mathbf{F}}\ \mathbf{\Delta S} + \overline{\mathbf{S}}\ \mathbf{\Delta F} \tag{41}$$

Where

$$\overline{\mathbf{F}} = \begin{bmatrix} F_{rr} & 0 & 0 & F_{rz} \\ 0 & F_{\theta\theta} & 0 & 0 \\ 0 & 0 & F_{zz} & F_{zr} \\ F_{zr} & 0 & 0 & F_{zz} \\ 0 & 0 & F_{rz} & F_{rr} \end{bmatrix},$$

$$,\overline{\mathbf{S}} = \begin{bmatrix} S_{rr} & 0 & 0 & S_{rz} \\ 0 & S_{\theta\theta} & 0 & 0 \\ 0 & 0 & S_{zz} & 0 \\ 0 & 0 & S_{rz} & 0 \\ S_{zr} & 0 & 0 & S_{zz} \end{bmatrix} \tag{42}$$

$$\mathbf{F} = \begin{Bmatrix} F_{rr} \\ F_{\theta\theta} \\ F_{zz} \\ F_{rz} \\ F_{zr} \end{Bmatrix},\ \ \mathbf{P} = \begin{Bmatrix} P_{rr} \\ P_{\theta\theta} \\ P_{zz} \\ P_{rz} \\ P_{zr} \end{Bmatrix},\ \ \mathbf{S} = \begin{Bmatrix} S_{rr} \\ S_{\theta\theta} \\ S_{zz} \\ S_{rz} \end{Bmatrix} \tag{43}$$

It should be mentioned that the second Piola-Kirchhoff stress tensor is symmetric (i.e., '$S_{rz} = S_{zr}$'). Substitution of Eqs. (10) and (17) into Eq. (41) leads us to the increment of 1st Piola-Kirchhoff stress in terms of nodal displacements.

$$\mathbf{\Delta P} = \left(\overline{\mathbf{F}}\, \mathbf{D}\, \mathbf{B}^{nl} + \overline{\mathbf{S}}\ \mathbf{B}^{l}\right) \mathbf{\Delta u} \tag{44}$$

Finally, by substituting Eq. (44) into Eq. (39), the incremental discretized equation of motion for node "$I$" can be obtained as:

$$\begin{aligned} &\left( \int_{\Omega_{Q_0}} \mathbf{W}' \left(\overline{\mathbf{F}}\, \mathbf{D}\, \mathbf{B}^{nl} + \overline{\mathbf{S}}\ \mathbf{B}^{l}\right) d\Omega_Q - \right. \\ &\left. \int_{\Gamma^i_{Q_0}+\Gamma^u_{Q_0}} r\, \mathbf{W}\, \mathbf{N} \left(\overline{\mathbf{F}}\, \mathbf{D}\, \mathbf{B}^{nl} + \overline{\mathbf{S}}\ \mathbf{B}^{l}\right) d\Gamma_Q \right) \mathbf{\Delta u} + \\ &\left( \int_{\Omega_{Q_0}} r\, \rho_0\, \mathbf{W}\ d\Gamma_Q \right) \mathbf{\Delta \ddot{u}} \\ &= \int_{\Gamma^t_{Q_0}} r\, \mathbf{W}\, \overline{\mathbf{T}}\ d\Gamma_Q - \int_{\Omega_{Q_0}} \mathbf{W}'\ \mathbf{P}_t\, d\Omega_Q + \\ &\int_{\Gamma^i_{Q_0}+\Gamma^u_{Q_0}} r\, \mathbf{W}\, \mathbf{N}\, \mathbf{P}_t\ d\Gamma_Q - \int_{\Omega_{Q_0}} r\, \rho_0\, \mathbf{W}\, \ddot{\mathbf{u}}_t\, d\Gamma_Q \end{aligned} \tag{45}$$

It can be found that Eq. (45) is nonlinear because both sides of this equation are a function of displacements. By considering the Rayleigh damping matrix '$\mathbf{C}$', the last equation can be rewritten in the following compact form:

$$\mathbf{K_T}\, \mathbf{\Delta u} + \mathbf{C} \mathbf{\Delta \dot{u}} + \mathbf{M} \mathbf{\Delta \ddot{u}} = \mathbf{\Delta P} \tag{46}$$

The incremental-iterative Newmark/Newton-Raphson technique is used to solve the last equation.

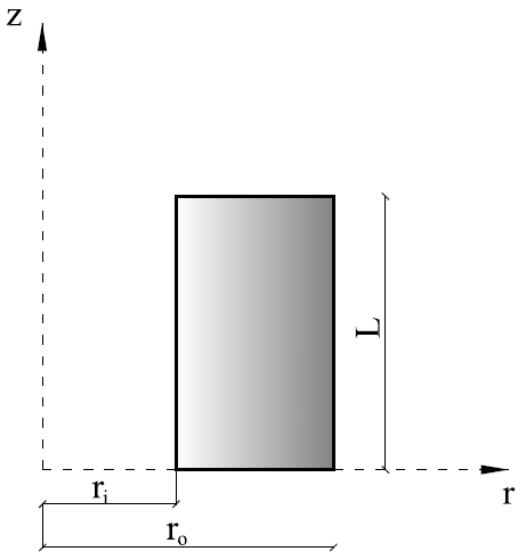


**Fig. 2. Schematics of the hollow cylinder.**

## 6- Numerical Examples and Discussion

### 6- 1- 6.1. Thick hollow cylinder under uniform internal pressure

In the first example, a homogeneous thick hollow cylinder with the following mechanical properties has been analyzed using the proposed method.

$$r_i = 0.25\,m,\ r_o = 0.5\,m,\ L = 0.5\,m,\ E = 2.75\,GPa,\ \nu = 0.3 \tag{47}$$

Where, '$r_i$', '$r_o$' and '$L$' are the inner radius, outer radius, and length of the cylinder (Fig. 2).

The cylinder is considered under the following dynamic internal pressure in the radial direction.

$$S_{rr}(r = r_i) = P_0\left(1 - e^{-ct}\right) \tag{48}$$

Where $P_0 = 20\,MPa$ and $c = 100\,s^{-1}$. According to Eq. (48) in a long-time limit, the internal pressure turns into a static pressure '$P_0$' and the dynamic behavior of the cylinder converges to steady-state. By considering these assumptions, it is possible to compare the obtained results with the analytical solution given by [29]:

$$u_r = r\left[\frac{P_0 r_i^2 (1+\nu)(1-2\nu)}{E\left(r_o^2 - r_i^2\right)}\right] + \frac{1}{r}\left[\frac{P_0 r_i^2 r_o^2 (1+\nu)}{E\left(r_o^2 - r_i^2\right)}\right] \tag{49}$$

The radial displacement along the cylinder thickness obtained from the MLPG method with various nodal distributions at a long time ($t = 100\,s$) is compared with the analytical result (obtained from Eq. (49)) in Fig. 3. It can be observed from this figure that in nodal distribution '16×24', the results convergence is achieved.

As the next example, an FG thick hollow cylinder with the following mechanical properties is linearly analyzed to show the accuracy and potentialities of the MLPG method.

$$r_i = 0.25\,m,\ r_o = 0.5\,m,\ L = 0.5\,m,\ n_r = 0.01,\ n_z = 0,\ \xi = 0 \tag{50}$$

To verify the obtained results, the same boundary conditions as that introduced in Hosseini et al. [27] reference, are considered for the problem.

$$S_{rr}(r = r_i) = \begin{cases} P_0\,t & t \le 0.005 \\ 0 & t > 0.005 \end{cases},\quad u_z = 0 \quad at\ z = 0 \tag{51}$$

where '$P_0 = 4GPa/s$'. In Fig. 4 the time history of radial displacement obtained by the presented MLPG method is compared with those obtained by the FEM method reported by Hosseini et al. [27]. As can be seen in this figure, an excellent agreement with the FEM solution is achieved.

Fig. 5 depicts the geometrically nonlinear time history of radial displacement of a cylinder with '$r_i = 0.3\,m$', '$r_o = 0.4\,m$', '$n_r = 0.01$', '$n_z = 0$', '$\xi = 0$' and linear constitutive model, under uniform external pressure. Rad et al. [28] analyzed the aforementioned cylinder supposing the plane strain conditions. In this paper, the length of the cylinder is considered to be very long '$L = 2\,m$' and the same boundary conditions introduced in Eq. (51) with '$P_0 = 700GPa/s$' are imposed at the cylinder ends. According to Fig. 5, the comparison between the results shows an acceptable agreement.

### 6- 2- Thick hollow cylinder under non-uniform internal pressure

Compared to Ref. [28] which deals with the time history analysis of cylinders with infinite length (plain strain condition) and variation of material properties only in the radial direction, this work-study the thick hollow cylinders in a more general case (limited length) which allows the two-dimensional wave propagation analysis of thick hollow cylinders made of 2D functionally graded materials. Thus, in this paper, a finite length cylinder with the $r_i = 0.25\,m$, $r_o = 0.5\,m$, $L = 0.5\,m$ dimensions and following boundary conditions is considered.

$$S_{rr}(r = r_i) = \begin{cases} P_0\,t & t \le 0.0025 \ \text{and}\ 0 \le z \le L/3 \\ 0 & t > 0.0025 \ \text{or}\ z > L/3 \end{cases} \tag{52}$$

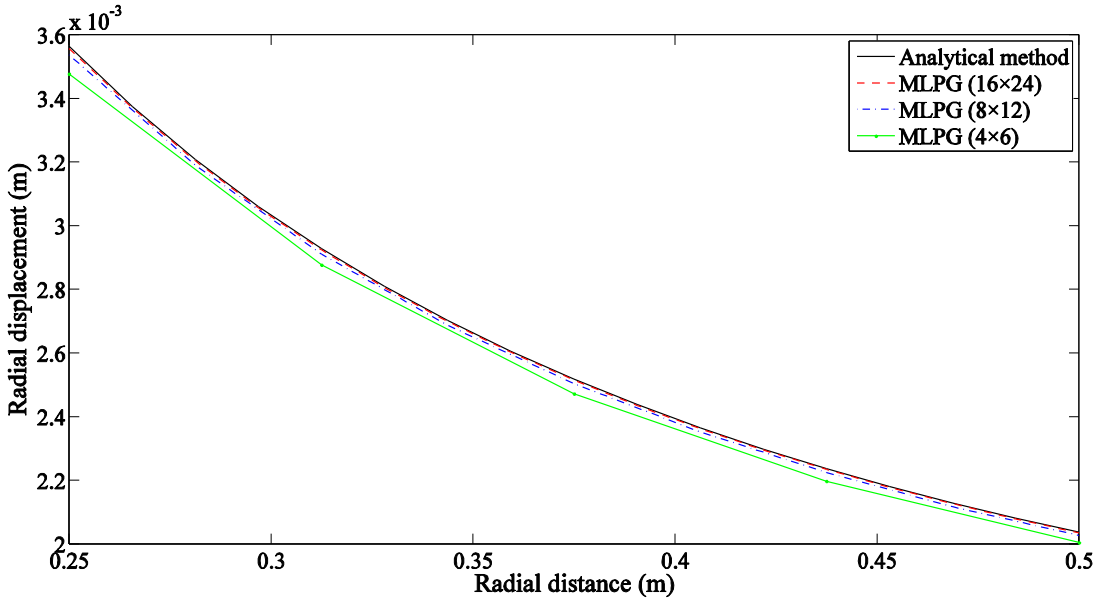


**Fig. 3. The convergence analysis of the proposed MLPG method.**

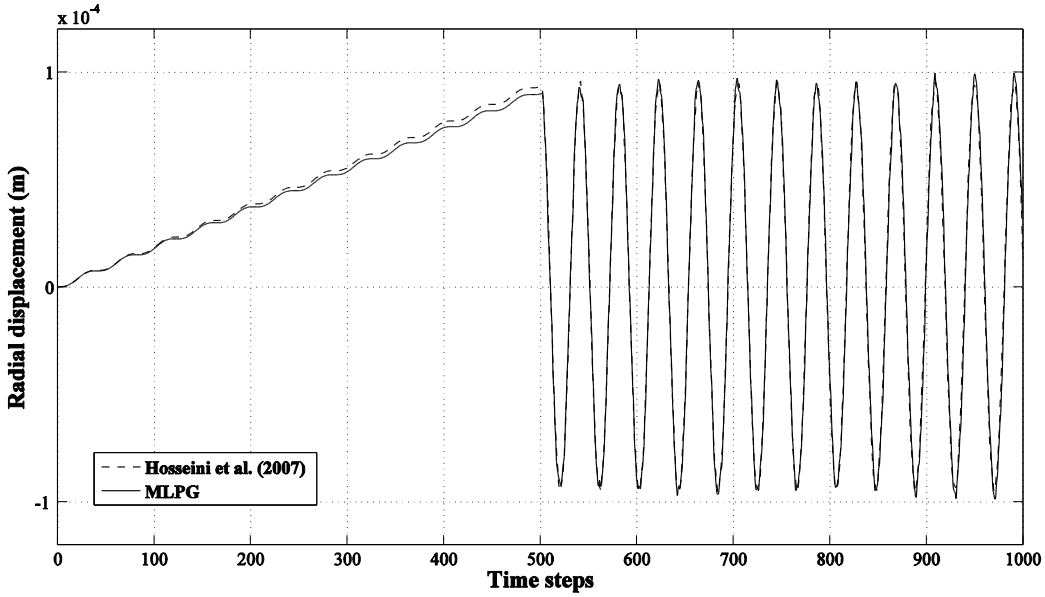


**Fig. 4. The linear radial displacement time history at the middle point of cylinder thickness under uniform internal pressure compared to FEM results reported in Hosseini et al.'s paper [27].**

Where '$P_0 = 6000GPa/s$'.

Fig. 6 depicts the linear 2D radial displacement contours for '$n_r = n_z = 0$' and '$\xi = 0.05$' at various times. The rate of contour changes at time intervals indicates the wave propagation speed.

The nonlinear radial displacement wave propagation of the 2D-FG cylinder with the same conditions and considering linear and neo-Hookean constitutive models can be tracked in Figs. 7 and 8, respectively. By comparison the Figs. 6 to 8 it can be found that the wave propagation speed in the linear and nonlinear analysis is almost identical. However, the values of radial displacement contours in nonlinear analysis with the linear constitutive model are less than linear analysis and in nonlinear analysis with the neo-Hookean constitutive model are more than linear analysis, at the high load steps ($t \geq 2e-4s$).

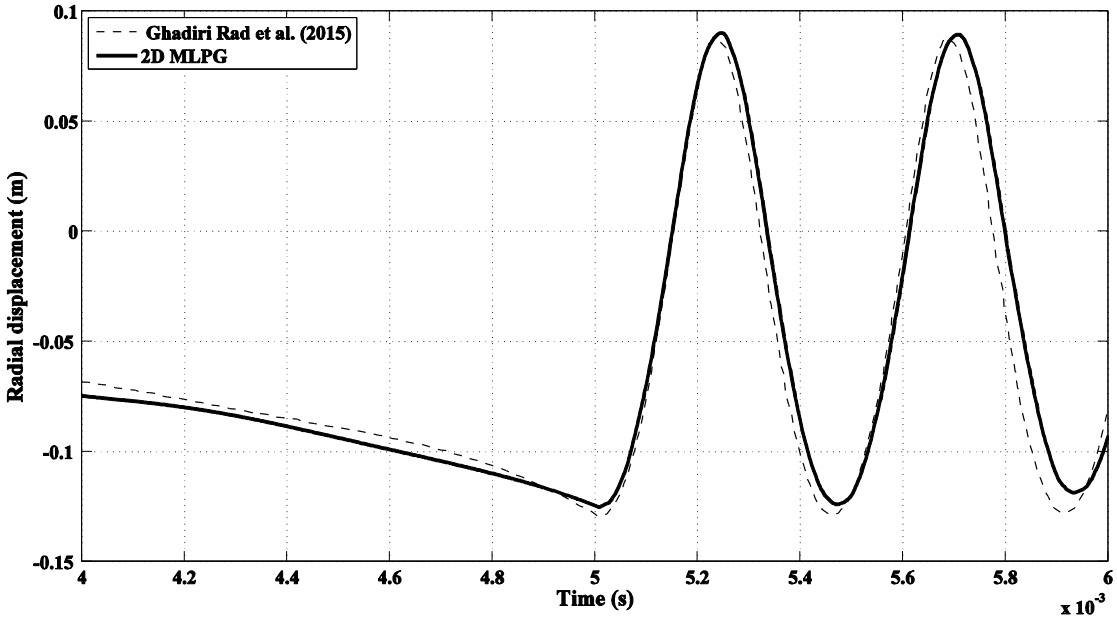


**Fig. 5. The nonlinear radial displacement time history at the middle point of thickness under uniform external pressure compared to results reported in Rad et al.'s paper [28].**

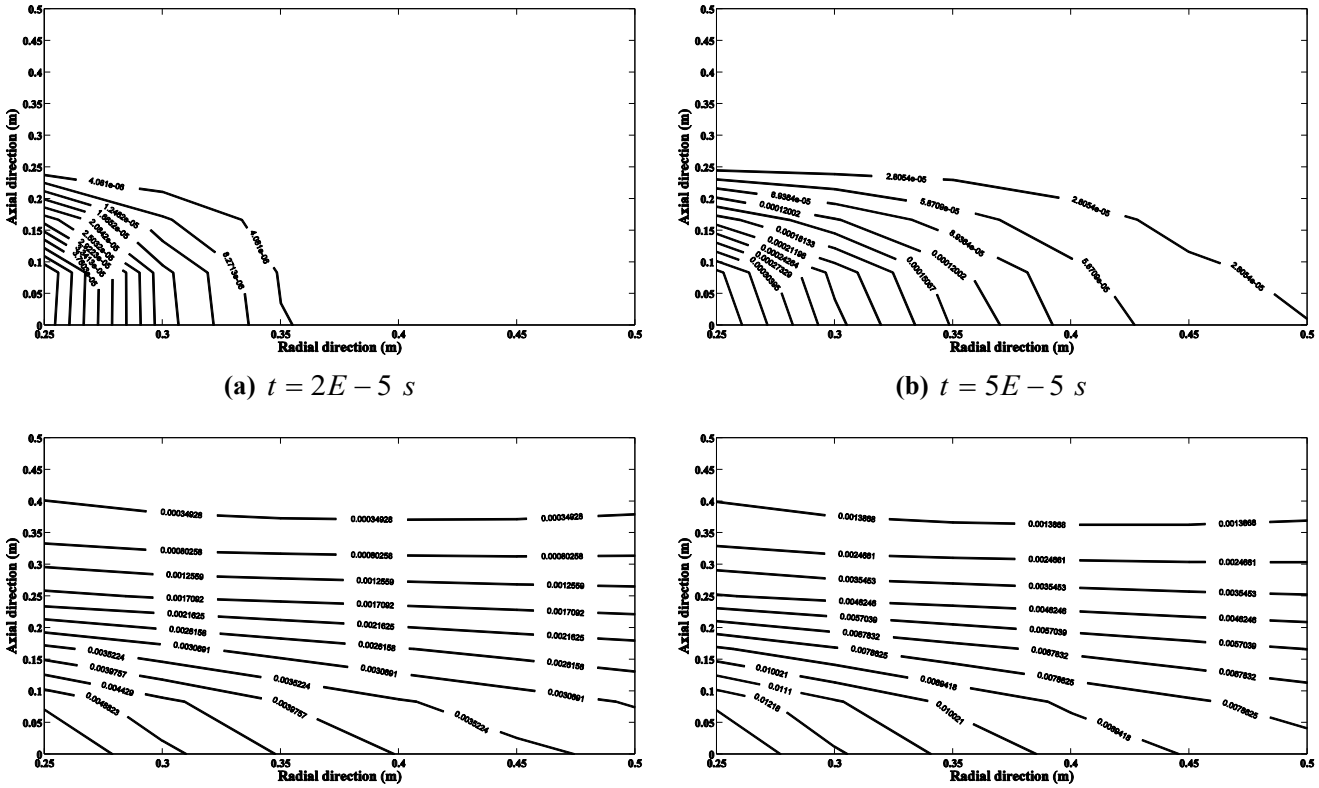


**(a)** $t = 2E-5\ s$ **(b)** $t = 5E-5\ s$

**(c)** $t = 2E-4\ s$ **(d)** $t = 5E-4\ s$

**Fig. 6. The 2D propagation of linear radial displacement wave for ' $n_r = n_z = 0$ ' and ' $\xi = 0.05$ ' at various times.**

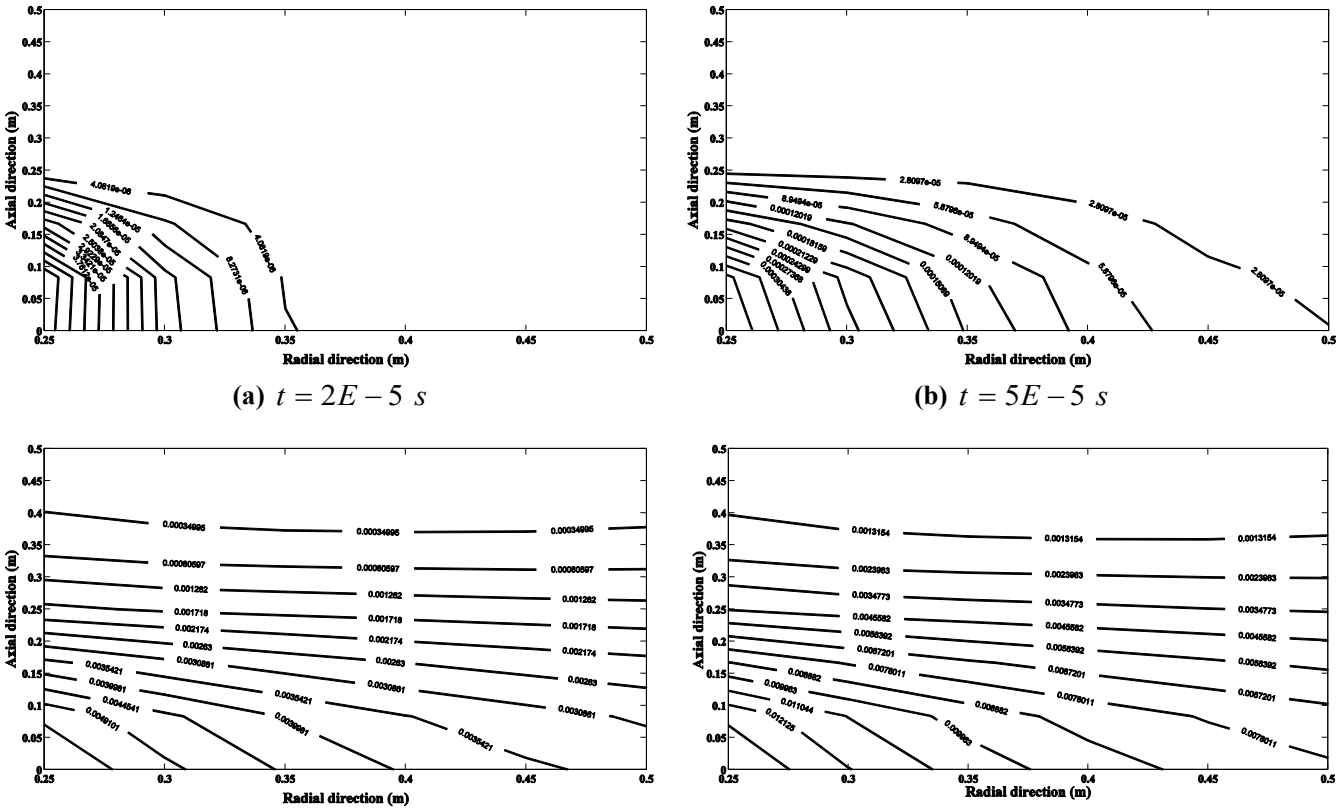


**Fig. 7. The 2D propagation of nonlinear radial displacement wave for ' $n_r = n_z = 0$ ', ' $\xi = 0.05$ ' and linear constitutive model at various times.**

The influence of the value of radial and longitudinal volume fraction exponents ' $n_r$ ' and ' $n_z$ ' on nonlinear wave propagation can be studied in Figs. 9 and 10, respectively. According to Fig. 9, it can be found that the radial volume fraction exponent has a significant effect on wave propagation speed so that by increasing the value of radial volume fraction exponent, the wave propagation speed is increased and values of radial displacement contours are decreased. Fig. 10 shows that when the value of longitudinal volume fraction exponent is increased; the values of radial displacement contours at any time step are decreased. But the influence of longitudinal volume fraction exponent on wave propagation speed is negligible.

The time history of nonlinear radial displacement at ' $z = L/2$ ' and the middle point of the cylinder thickness for various damping ratios ' $\xi$ ' are plotted in Fig. 11. This figure shows that in the typical range of damping ' $\xi \le 20\%$ ', the most important effect of the damping ratio is on the rate of vibration decays in the free vibration part. In the other words, the rate of vibration decays will be increased by increasing the damping ratio.

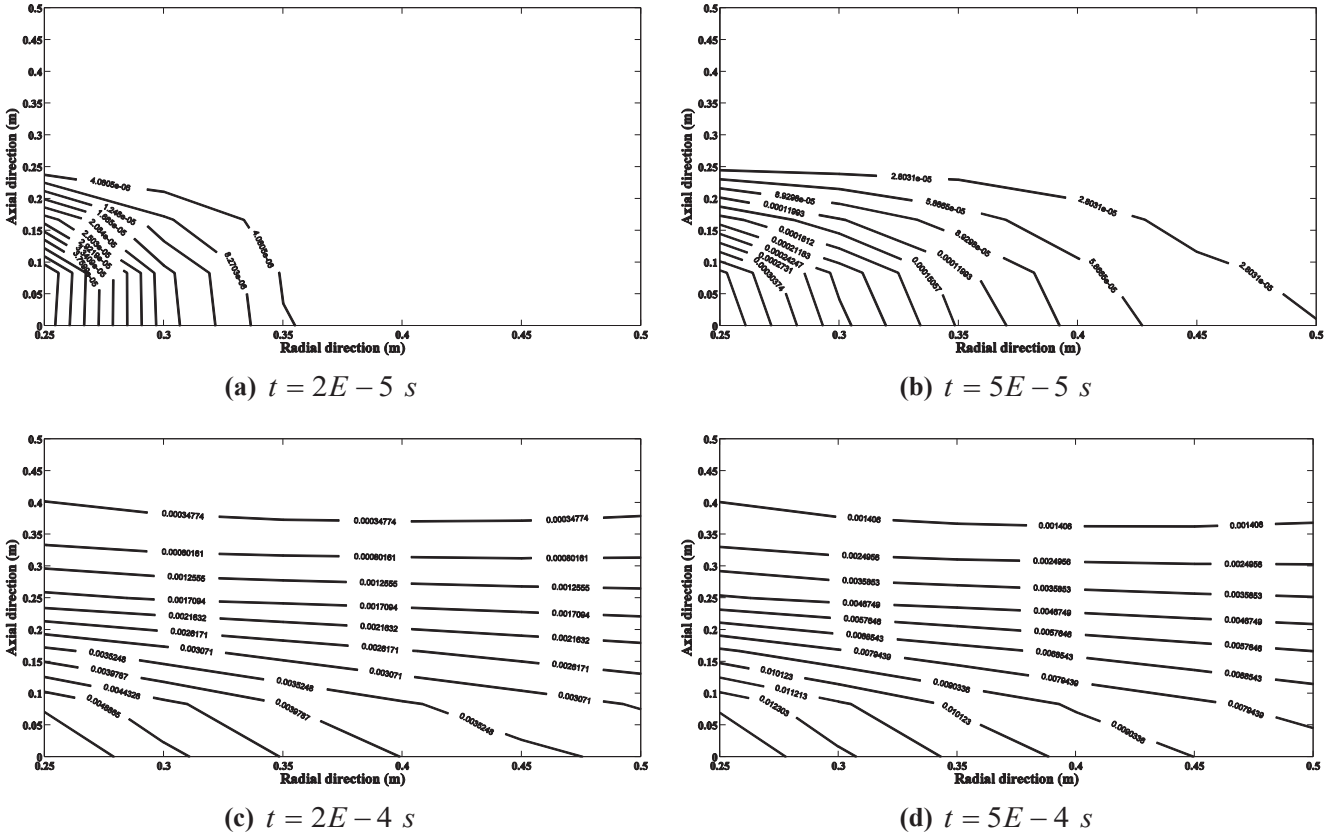


**(a)** $t = 2E-5\ s$ **(b)** $t = 5E-5\ s$

**(c)** $t = 2E-4\ s$ **(d)** $t = 5E-4\ s$

**Fig. 8. The 2D propagation of nonlinear radial displacement wave for ' $n_r = n_z = 0$ ', ' $\xi = 0.05$ ' and neo-Hookean constitutive model at various times**

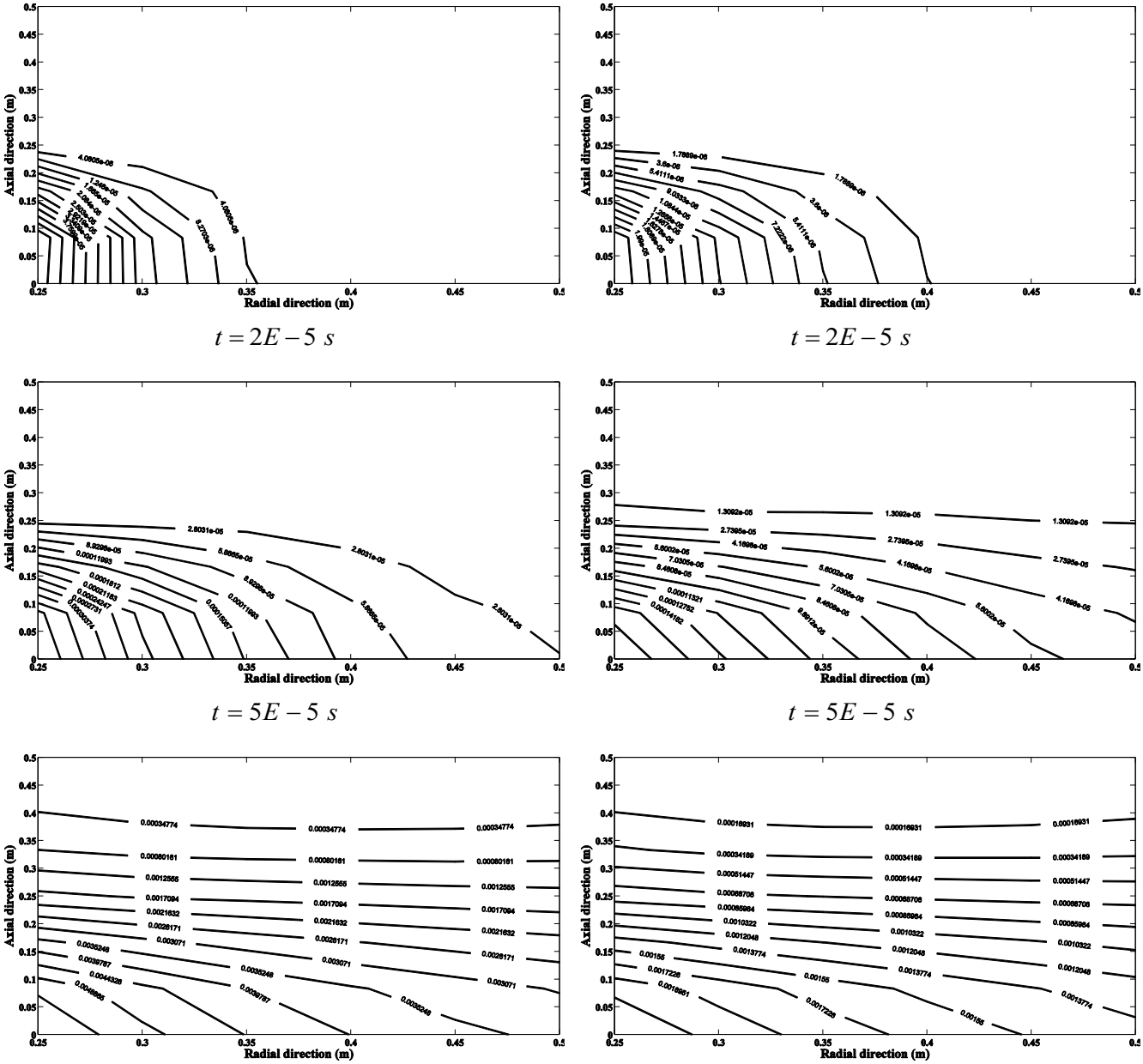


**(a)** $n_r = 0$ **(b)** $n_r = 1$

**Fig. 9. The 2D propagation of nonlinear radial displacement wave for $n_z = 0$ ' ' and various ' $n_r$ '.**

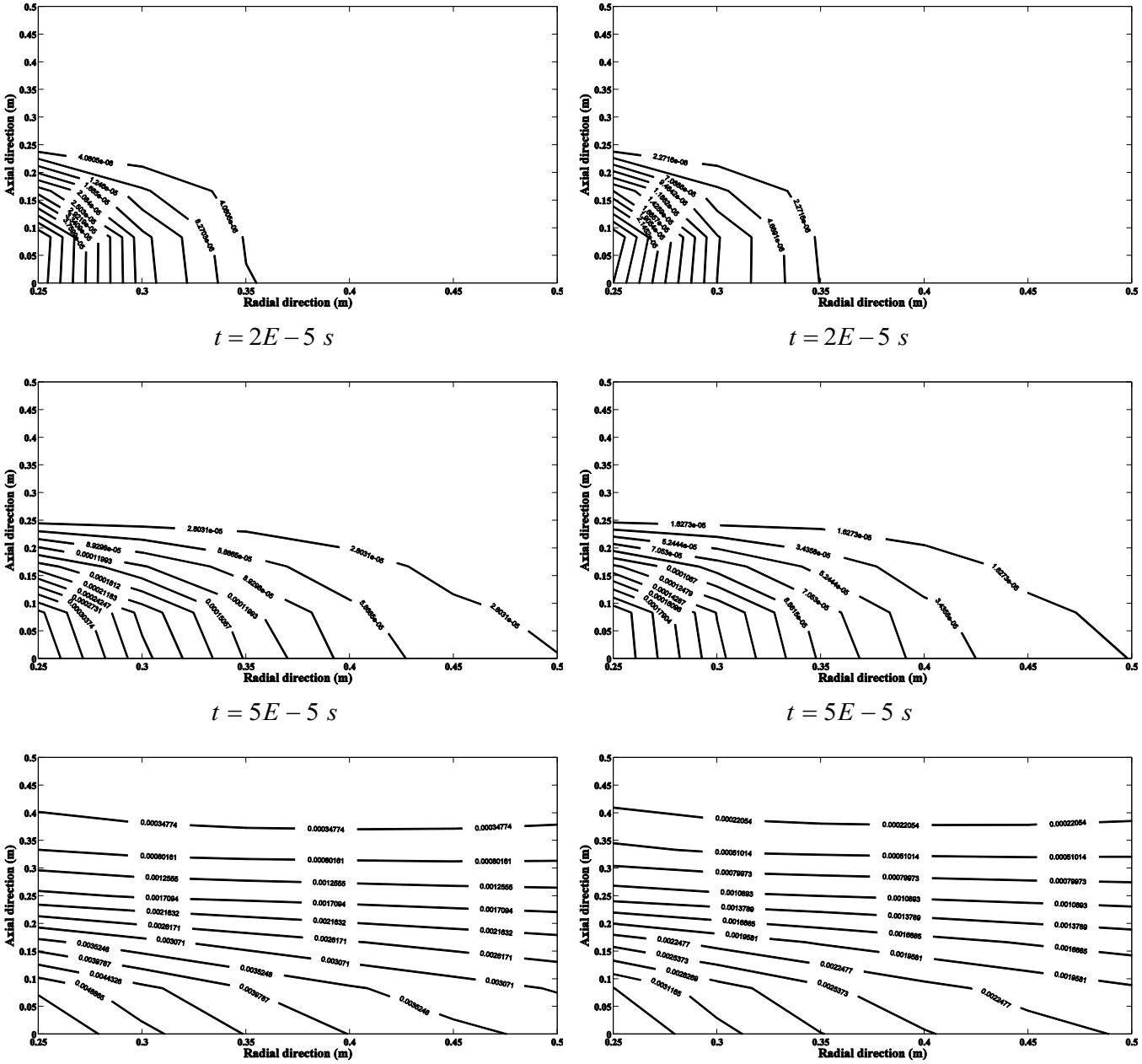


**(a)** $n_z = 0$ **(b)** $n_z = 1$

**Fig. 10. The 2D propagation of nonlinear radial displacement wave for '** $n_r = 0$ **' and various '** $n_z$ **'.**

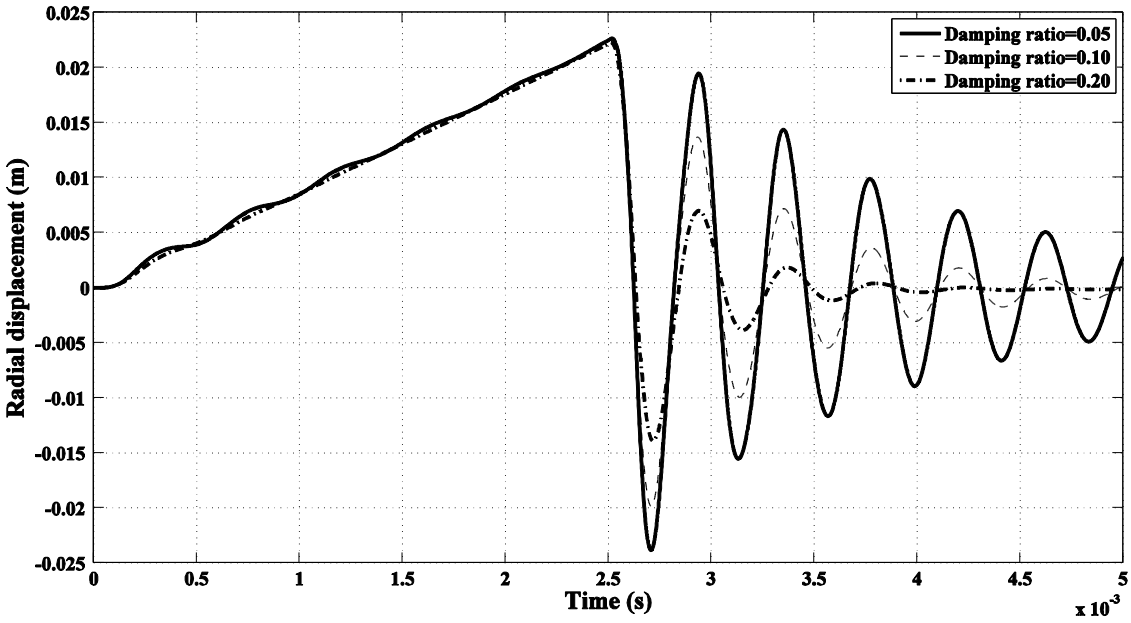


**Fig. 11. Time history of radial displacement at the middle point of cylinder thickness for various values of damping ratios.**

## 7- Conclusion

The main objective of this study is to develop an MLPG technique for geometrically nonlinear analysis of 2D-FG hollow cylinders with finite deformations. Because of large deformations, the neo-Hookean hyperelastic model is applied for the constitutive law. The material properties are simulated using two-dimensional volume fractions. In the present work, the iterative Newmark/ Newton-Raphson algorithm is employed to solve time-dependent nonlinear systems of equations. The hollow cylinder is analyzed under uniform and non-uniform mechanical shock loading. Several numerical examples are presented and effects of relative parameters such as constitutive model, radial and longitudinal volume fractions, and damping ratios on wave propagation are discussed in detail. Through the current research the following conclusions can be drawn:

- The accuracy and potentialities of the present method for analysis of thick hollow cylinder have been successfully demonstrated by verifying with the FEM results.
- A comparison between the results of linear and nonlinear analyses shows that the wave propagation speed in the linear and nonlinear analyses is almost identical.
- The values of radial displacement contours in nonlinear analysis with the linear constitutive model are less than a linear solution at the high time steps. The values of radial displacement contours in nonlinear analysis with the neo-Hookean constitutive model are more than linear solution at the high time steps.
- The peak points in time histories of nonlinear radial displacement with linear and neo-Hookean constitutive models are less and more than the linear radial displacement, respectively.
- The effects of volume fraction on wave propagation are studied and it is concluded that by increasing the value of radial volume fraction exponent, the wave propagation speed is increased but the values of radial displacement contours are decreased. Increasing the value of longitudinal volume fraction exponent has no significant effect on wave propagation speed but causes to decrease in the values of radial displacement contours.
- The most important effect of the damping ratio is on the rate of vibration decays in the free vibration part. So that by increasing the damping ratio, the rate of vibration decays will be increased.

## References

[1] S. Moussavinezhad, F. Shahabian, S.M. Hosseini, Two-dimensional stress-wave propagation in finite-length FG cylinders with two-directional nonlinear grading patterns using the MLPG method, Journal of Engineering Mechanics, 140(3) (2014) 575-592.

[2] A. Norouzzadeh, R. Ansari, H. Rouhi, An analytical study on wave propagation in functionally graded nano-beams/tubes based on the integral formulation of nonlocal elasticity, Waves in Random and Complex Media, 30(3) (2020) 562-580.

[3] Sur, S. Paul, M. Kanoria, Modeling of memory-dependent derivative in a functionally graded plate, Waves in Random and Complex Media, 31(4) (2021) 618-638.

[4] H. Aminipour, M. Janghorban, L. Li, Wave dispersion in nonlocal anisotropic macro/nanoplates made of functionally graded materials, Waves in Random and Complex Media, (2020) 1-45.

[5] A. Khoei, M. Anahid, K. Shahim, An extended arbitrary Lagrangian-Eulerian finite element method for large deformation of solid mechanics, Finite Elements in Analysis and Design, 44(6-7) (2008) 401-416.

[6] M. Schwarze, S. Reese, A reduced integration solid-shell finite element based on the EAS and the ANS concept-geometrically linear problems, International Journal for Numerical Methods in Engineering, 80(10) (2009) 1322-1355.

[7] M. Rezaiee-Pajand, A.R. Masoodi, E. Arabi, Geometrically nonlinear analysis of FG doubly-curved and hyperbolical shells via laminated by new element, Steel and Composite Structures, 28(3) (2018) 389-401.

[8] P.C. Guan, C.T. Sun, The isoparametric reproducing kernel particle method for nonlinear deformation of plates, Engineering Analysis with Boundary Elements, 42 (2014) 67-76.

[9] R.A. Gingold, J.J. Monaghan, Smoothed particle hydrodynamics: theory and application to non-spherical stars, Monthly Notices of the royal astronomical society, 181(3) (1977) 375-389.

[10] Nayroles, G. Touzot, P. Villon, Generalizing the finite element method: diffuse approximation and diffuse elements, Computational Mechanics, 10(5) (1992) 307-318.

[11] W.K. Liu, S. Jun, S. Li, J. Adee, T. Belytschko, Reproducing kernel particle methods for structural dynamics, International Journal for Numerical Methods in Engineering, 38(10) (1995) 1655-1679.

[12] T. Belytschko, Y.Y. Lu, L. Gu, Element-free Galerkin methods, International journal for numerical methods in engineering, 37(2) (1994) 229-256.

[13] Yongchang, Z. Hehua, A meshless local natural neighbor interpolation method for stress analysis of solids, Engineering analysis with boundary elements, 28(6) (2004) 607-613.

[14] S.N. Atluri, T. Zhu, A new meshless local Petrov-Galerkin (MLPG) approach in computational mechanics, Computational Mechanics, 22(2) (1998) 117-127.

[15] S.N. Atluri, J. Sladek, V. Sladek, T. Zhu, The local boundary integral equation (LBIE) and its meshless implementation for linear elasticity, Computational mechanics, 25(2-3) (2000) 180-198.

[16] J. Sladek, V. Sladek, C. Zhang, F. Garcia-Sanchez, M. Wunsche, Meshless local Petrov-Galerkin method for plane piezoelectricity, CMC: Computers, Materials & Continua, 4(2) (2006) 109-117.

[17] Y. Hao, W. Zhang, J. Yang, Nonlinear dynamics of an FGM plate with two clamped opposite edges and two free edges, Acta Mechanica Solida Sinica, 27(4) (2014) 394-406.

[18] J. Sladek, V. Sladek, S. Krahulec, E. Pan, The MLPG analyses of large deflections of magnetoelectroelastic plates, Engineering Analysis with Boundary Elements, 37(4) (2013) 673-682.

[19] G. Zhang, A. Wittek, G. Joldes, X. Jin, K. Miller, A three-dimensional nonlinear meshfree algorithm for simulating mechanical responses of soft tissue, Engineering Analysis with Boundary Elements, 42 (2014) 60-66.

[20] L. Zhang, Z. Lei, K. Liew, J. Yu, Large deflection geometrically nonlinear analysis of carbon nanotube-reinforced functionally graded cylindrical panels, Computer Methods in Applied Mechanics and Engineering, 273 (2014) 1-18.

[21] X. Zhao, Y. Yang, K.M. Liew, Geometrically nonlinear analysis of cylindrical shells using the element-free kp-Ritz method, Engineering Analysis with Boundary Elements, 31(9) (2007) 783-792.

[22] P. Zhu, L. Zhang, K. Liew, Geometrically nonlinear thermomechanical analysis of moderately thick functionally graded plates using a local Petrov–Galerkin approach with moving Kriging interpolation, Composite Structures, 107 (2014) 298-314.

[23] M.H. Ghadiri Rad, F. Shahabian, S.M. Hosseini, Nonlocal geometrically nonlinear dynamic analysis of nanobeam using a meshless method, Steel and Composite Structures, 32(3) (2019) 293-304.

[24] H. Mellouli, H. Jrad, M. Wali, F. Dammak, Geometrically nonlinear meshfree analysis of 3D-shell structures based on the double directors shell theory with finite rotations, Steel and Composite Structures, 31(4) (2019) 397-408.

[25] G. Liu, Y. Gu, A local radial point interpolation method (LRPIM) for free vibration analyses of 2-D solids, Journal of Sound and Vibration, 246(1) (2001) 29-46.

[26] Y. Gu, Q. Wang, K. Lam, A meshless local Kriging method for large deformation analyses, Computer Methods in Applied Mechanics and Engineering, 196(9-12) (2007) 1673-1684.

[27] S.M. Hosseini, M. Akhlaghi, M. Shakeri, Dynamic response and radial wave propagation velocity in thick hollow cylinder made of functionally graded materials, Engineering Computations, 24(3) (2007) 288-303.

[28] M.H.G. Rad, F. Shahabian, S.M. Hosseini, Geometrically nonlinear elastodynamic analysis of hyper-elastic neo-Hooken FG cylinder subjected to shock loading using MLPG method, Engineering Analysis with Boundary Elements, 50 (2015) 83-96.

[29] V. Vullo, Circular cylinders and pressure vessels. Stress Analysis and Design, Springer: Berlin/Heidelberg, Germany, 2014.

**HOW TO CITE THIS ARTICLE**

*M.H. Ghadiri Rad, F. Shahabian , S.M. Hosseini, Two-Dimensional Geometrically Nonlinear Hyperelastic Wave Propagation Analysis in FG Thick Hollow Cylinders using MLPG Method , AUT J. Civil Eng., 5(3) (2021) 465-480.*

**DOI:** 10.22060/ajce.2021.19911.5752